Inorg. Chem. **2006**, *45*, 10197–10206

$[Mn_7O_5(OR)_2(O_2CPh)_9(terpy)]$ (R = Me, CH_2Ph) Complexes with a Fused Cubane/Butterfly Core and an $S = 6$ Ground-State Spin

Abhudaya Mishra,[†] Wolfgang Wernsdorfer,[‡] Khalil A. Abboud,[†] and George Christou*[,†]

Department of Chemistry, University of Florida, Gainesville, Florida 32611-7200, and Laboratoire Louis Néel-CNRS, BP 166, 25 Avenue des Martyrs, 38042 Grenoble Cedex 9, France

Received July 18, 2006

Two new heptanuclear Mn clusters, $[Mn_7O_5(OMe)_2(O_2CPh)_9(terpy)]$ (**1**) and $[Mn_7O_5(OCH_2Ph)_2(O_2CPh)_9(terpy)]$ (**2**), were prepared from the partial alcoholysis of the trinuclear complex $[Mn_3O(O_2CPh)_6(py)_2(H_2O)]$ (**3**) in the presence of terpy (terpy = 2,2′:6′,2″-terpyridine). Complexes **1** and **2** crystallize in the triclinic $P\bar{1}$ and the orthorhombic *Pbca* space groups, respectively. The clusters are both mixed valent, containing three Mn oxidation states: Mn^{IV}, $5Mn^{III}$, and Mn^{II}. The Mn ions are held together by nine doubly bridging benzoates, four μ_3-O^{2-} ions, one μ_5-O^{2-} ion, and either two μ-MeO^- (**1**) or two μ-$PhCH_2O^-$ (**2**) groups. The single terpy chelate in each complex is attached to the Mn^{II} ion. The core topology is novel and very unusual, comprising a cubane and a butterfly unit fused by sharing a Mn^{III} and the μ_5-O^{2-} ion. Solid-state dc and ac magnetic susceptibility studies establish that complexes **1** and **2** both possess an $S = 6$ ground-state spin. Fits of variable-temperature and -field magnetization data gave $S = 6$, $g = 1.88$, and $D = -0.21$ cm^{-1} for **1** and $S = 6$, $g = 1.86$, and $D = -0.18$ cm^{-1} for **2**. Single-crystal magnetization vs dc field scans down to 0.1 K for **2** show only very little hysteresis at 0.1 K.

Introduction

One of the motivating themes in multinuclear cluster chemistry research is the design of high-nuclearity manganese carboxylate clusters that can function as nanoscale magnetic materials. Such species display superparamagnet-like, slow relaxation of the magnetization vector below their blocking temperature (T_B) and have been termed single-molecule magnets (SMMs). Such molecules function as magnets, exhibiting hysteresis in magnetization versus dc field scans. Since SMMs are, by definition, molecular in nature, they thus represent a molecular, or bottom-up, approach to nanomagnetism.[1] The magnetic behavior of SMMs results from the combination of a large ground spin state (S) with a large and negative (Ising or easy-axis) magnetoanisotropy, as measured by the axial zero-field (ZFS) splitting parameter D. This leads to a significant barrier (U) to magnetization reversal, its maximum value given by $S^2|D|$ or $(S^2 - 1/4)|D|$ for integer and half-integer spin, respectively.[1,2] However, in practice, quantum tunneling of the magnetization (QTM) through the barrier via higher lying M_S levels of the spin S manifold results in the actual or effective barrier (U_{eff}) being less than U.

* To whom correspondence should be addressed. Phone: (352) 392-8314. Fax: (352) 392-8757. E-mail: christou@chem.ufl.edu.
[†] University of Florida.
[‡] Laboratoire Louis Néel-CNRS.

(1) (a) Christou, G.; Gatteschi, D.; Hendrickson, D. N., Sessoli, R. *MRS Bull.* **2000**, *25*, 66 and references therein. (b) Aromi, G.; Aubin, S. M. J.; Bolcar, M. A.; Christou, G.; Eppley, H. J.; Folting, K.; Hendrickson, D. N.; Huffman, J. C.; Squire, R. C.; Tsai, H. -L.; Wang, S.; Wemple, M. W. *Polyhedron* **1998**, *17*, 3005. (c) Christou, G. *Polyhedron* **2005**, *24*, 2065. (d) Brechin, E. K. *Chem. Commun*. **2005**, 5141.

(2) (a) Sessoli, R.; Gatteschi, D.; Caneschi, A.; Novak, M. A. *Nature* **1993**, *365*, 141. (b) Sessoli R.; Ysai, H. -L.; Schake, A. R.; Wang, S.; Vincent, J. B.; Folting, K.; Gatteschi, D.; Christou, G.; Hendrickson, D. N. *J. Am. Chem. Soc.* **1993**, *115*, 1804. (c) Thomas, L.; Lionti, L.; Ballou, R.; Gatteschi, D.; Sessoli, R.; Barbara, B. *Nature* **1996**, 383, 145.

(3) (a) Eppley, H. J.; Tsai, H.-L.; de Vries, N.; Folting, K.; Christou, G.; Hendrickson, D. N. *J. Am. Chem. Soc*. **1995**, *117*, 301. (b) Aubin, S. M. J.; Spagna, S.; Eppley, H. J.; Sager, R. E.; Christou, G.; Hendrickson, D. N. *Chem. Commun.* **1998**, 803. (c) Aubin, S. M. J.; Sun, Z.; Pardi, L.; Krzystek, J.; Folting, K.; Brunel, L.-C.; Rheingold, A. L.; Christou, G.; Hendrickson, D. N. *Inorg. Chem.* **1999**, *38*, 5329. (d) Soler, M.; Chandra, S. K.; Ruiz, D.; Davidson, E. R.; Hendrickson, D. N.; Christou, G. *Chem. Commun.* **2000**, 2417. (e) Boskovic, C.; Pink, M.; Huffman, J. C.; Hendrickson, D. N.; Christou, G. *J. Am. Chem. Soc.* **2001**, *123*, 9914. (f) Artus, P.; Boskovic, C.; Yoo, J.; Streib, W. E.; Brunel, L.-C.; Hendrickson, D. N.; Christou, G. *Inorg. Chem.* **2001**, *40*, 4199. (g) Soler, M.; Wernsdorfer, W.; Abboud, K. A.; Huffman, J. C.; Davidson, E. R.; Hendrickson, D. N.; Christou, G. *J. Am. Chem. Soc*. **2003**, *125*, 3576. (h) Chakov, N. E.; Wernsdorfer, W.; Abboud, K. A.; Hendrickson, D. N.; Christou, G. *Dalton Trans.* **2003**, 2243. (i) Morello, A.; Bakharev, O. N.; Brom, H. B.; de Jongh, L. J. *Polyhedron* **2003**, *22*, 1745. (j) Bian, G. -Q.; Kuroda-Sowa, T.; Konaka, H.; Hatano, M.; Maekawa, M.; Munakata, M.; Miyasaka, H.; Yamashita, M. *Inorg. Chem*. **2004**, *43*, 4790.

10.1021/ic061334d CCC: $33.50
Published on Web 11/09/2006

The first SMM discovered was $[Mn_{12}O_{12}(O_2CMe)_{16}(H_2O)_4]$,[2] and synthetic manipulation of this complex has provided a very well studied family of related complexes.[2,3] Since the discovery of Mn_{12} complexes, several types of SMMs have been discovered, most of them containing primarily Mn^{III} ions.[4] This has allowed important insight into how the various structural, nuclearity, oxidation state, symmetry, and other variations between species affect the resultant magnetic and other properties of these clusters. In manganese carboxylate cluster chemistry, there have been detailed investigations, for example, of various Mn_4 motifs such as defect-dicubane,[5] cubane,[6] butterfly,[7] and adamantane[8] complexes. It is rare to find more complicated structural types that clearly are structural hybrids of two or more of these motifs, but this is what we have recently encountered and describe in the present paper. While developing new synthetic routes to polynuclear Mn species using the rigid tridentate chelate 2,2′:6′,2″-terpyridine (terpy), we have discovered two isostructural Mn_7 clusters that possess a very unusual Mn_7 core comprising a fused butterfly/cubane moiety. It is also a rare example of three oxidation states of Mn in the same molecule and has a spin ground state of significant magnitude, $S = 6$. We describe herein the syntheses and structural and magnetic characterization of these two complexes and additionally demonstrate that one of them displays magnetization hysteresis arising from slow magnetization relaxation.

Experimental Section

Syntheses. All manipulations were performed under aerobic conditions using chemicals as received, unless otherwise stated. $[Mn_3O(O_2CPh)_6(py)_2(H_2O)]$ (**3**)[9] and $(NBu^n_4)[Mn_4O_2(O_2CPh)_9(H_2O)]$ (**4**)[7a] were prepared as previously described.

$[Mn_7O_5(OMe)_2(O_2CPh)_9(terpy)]\cdot 5MeCN$ (1·5MeCN). Method A. To a slurry of **3** (0.50 g, 0.45 mmol) in MeCN/MeOH (20/2 mL) was added solid terpy (0.050 g, 0.23 mmol), and the mixture was stirred for 20 min. The resulting red-brown solution was filtered and the filtrate concentrated by slow evaporation to yield brown crystals of **1**·5MeCN within a couple of days. These were collected by filtration, washed well with acetone, and dried in vacuo. The yield was 60%. Anal. Calcd (Found) for **1**·5MeCN, $C_{90}H_{77}O_{25}N_8Mn_7$: C, 52.60 (52.55); H, 3.78 (3.72); N, 5.45 (5.40). Selected IR data (KBr, cm^{-1}): 3432(s, br), 1599(s), 1563(s), 1449(w), 1385(s), 1025(w), 772(w), 717(s), 681(m), 621(m), 542(w), 473(w).

Method B. Complex **4** (0.50 g, 0.31 mmol) and terpy (0.03 g, 0.12 mmol) were dissolved with stirring in MeCN/MeOH (20 mL/2 mL). After 20 min, the red-brown solution was filtered and the filtrate slowly concentrated by evaporation to yield brown crystals within a few days. These were collected by filtration, washed with acetone, and dried briefly in vacuo. The yield was 45%. The product was identified as **1**·5MeCN by IR spectral comparison with material from method A and elemental analysis. Anal. Calcd (Found) for **1**·5MeCN, $C_{90}H_{77}O_{25}N_8Mn_7$: C, 52.60 (52.62); H, 3.78 (3.82); N, 5.45 (5.49).

$[Mn_7O_5(OCH_2Ph)_2(O_2CPh)_9(terpy)]\cdot 5MeCN$ (2·5MeCN). Method A. To a stirred slurry of **3** (0.25 g, 0.23 mmol) in MeCN/$PhCH_2$OH (20 mL/1 mL) was added terpy (0.02 g, 0.07 mmol), and the mixture was stirred for a further 30 min. The resulting brown solution was filtered and the filtrate concentrated by slow evaporation to yield black crystals of **2**·5MeCN over the course of a week. These were collected by filtration, washed with acetone, and dried overnight in vacuo. The yield was 50%. Crystals dried overnight analyzed as solvent-free. Anal. Calcd (Found) for **2**, $C_{92}H_{70}O_{25}N_3Mn_7$: C, 55.19 (54.95); H, 3.52 (3.24); N, 2.10 (2.27). Selected IR data (KBr, cm^{-1}): 3440(s, br), 1599(s), 1562(s), 1450(w), 1370(s), 1024(w), 771(w), 717(s), 683(m), 628(m), 541(w), 472(w).

Method B. The same product **2** was obtained from a reaction that employed complex **4** instead of **3**, followed by workup as described in method A. The product was identified as **2** by IR spectral comparison with material from method A and elemental analysis. Anal. Calcd (Found) for **2**, $C_{92}H_{70}O_{25}N_3Mn_7$: C, 55.19 (55.10); H, 3.52 (3.45); N, 2.10 (2.20).

(4) (a) Miyasaka, H.; Clérac, R.; Wernsdorfer, W.; Lecren, L.; Bonhomme, C.; Sugiura, K.; Yamashita, M. A. *Angew. Chem., Int. Ed.* **2004**, *43*, 2801. (b) Milios, C. J.; Raptopoulou, C. P.; Terzis, A.; Lloret, F.; Vicente, R.; Perlepes, S. P.; Escuer, A. *Angew. Chem., Int. Ed.* **2003**, *43*, 210. (c) Brechin, E. K.; Soler, M.; Davidson, J.; Hendrickson, D. N.; Parsons, S.; Christou, G. *Chem. Commun.* **2002**, 2252. (d) Price, D. J.; Batten, S. R.; Moubaraki B.; Murray, K. S. *Chem. Commun.* **2002**, 762. (e) Brechin, E. K.; Boskovic, C.; Wernsdorfer, W.; Yoo, J.; Yamaguchi, A.; Sanudo, E. C.; Concolino, T. R.; Rheingold, A. L.; Ishimoto, H.; Hendrickson, D. N.; Christou, G. C. *J. Am. Chem. Soc.* **2002**, *124*, 9710. (f) Sanudo, E. C.; Wernsdorfer, W.; Abboud, K. A.; Christou, G. *Inorg. Chem.* **2004**, *43*, 4137. (g) Tasiopoulos, A. J.; Vinslava, A.; Wernsdorfer, W.; Abboud, K. A.; Christou, G. *Angew. Chem., Int. Ed.* **2004**, *43*, 2117. (h) Tasiopoulos, A. J.; Wernsdorfer, W.; Abboud, K. A.; Christou, G. *Angew. Chem., Int. Ed.* **2004**, *43*, 6338. (i) Zaleski, C. M.; Depperman, E. C.; Dendrinou-Samara, C.; Alexiou, M.; Kampf, J. W.; Kessissoglou, D. P.; Kirk, M. L.; Pecoraro, V. L. *J. Am. Chem. Soc.* **2005**, *127*, 12862.

(5) (a) Brechin, E.K.; Yoo, J.; Huffman, J. C.; Hendrickson D. N.; Christou, G. *Chem. Commun.* **1999**, 783. (b) Yoo, J.; Brechin, E. K.; Yamaguchi, A.; Nakano, M.; Huffman, J. C.; Maniero, A. L.; Brunel, L.-C.; Awaga, K.; Ishimoto, H.; Christou; G.; Hendrickson, D. N. *Inorg. Chem.* **2000**, *39*, 3615. (c) Yoo, J.; Yamaguchi, A.; Nakano, M.; Krzystek, J.; Streib, W. E.; Brunel, L.-C.; Ishimoto, H.; Christou G.; Hendrickson, D. N. *Inorg. Chem.* **2001**, *40*, 4604. (d) Lecren, L.; Wernsdorfer, W.; Li, Y.-G.; Roubeau, O.; Miyasaka, H.; Clerac, R. *J. Am. Chem. Soc.* **2005**, *127*, 11311. (e) Lecren, L.; Roubeau, O.; Coulon, C.; Li, Y.-G.; Le Goff, X. F.; Wernsdorfer, W.; Miyasaka, H.; Clerac, R. *J. Am. Chem. Soc.* **2005**, *127*, 17353.

(6) (a) Aubin, S. M. J.; Wemple, M. W.; Adams, D. M.; Tsai, H.-L.; Christou, G. and Hendrickson, D. N. *J. Am. Chem. Soc.* **1996**, *118*, 7746. (b) Wang, S.; Wemple, M. S.; Tsai, H.-L.; Folting, K.; Huffman, J. C.; Hagen, K. S.; Hendrickson, D. N.; Christou, G. *Inorg. Chem.* **2000**, *39*, 1501. (c) Aubin, S. M.; Gilley, N. R.; Pardi, L.; Krzystek, J.; Wemple, M. W.; Brunel, L. C.; Marple, M. B.; Christou, G.; Hendrickson, D. N. *J. Am. Chem. Soc.* **1998**, *120*, 4991. (d) Aliaga-Alcalde, N.; Edwards, R. S.; Hill, S. O.; Wernsdorfer, W.; Folting, K.; Christou, G. *J. Am. Chem. Soc.* **2004**, *126*, 12503. (e) Wu, J.-Z.; De Angelis, F.; Carrell, T. G.; Yap, G. P. A.; Sheats, J.; Car, R.; Dismukes, G. C. *Inorg. Chem.* **2006**, *45*, 189.

(7) (a) Wemple, M. W.; Tsai, H.-L.; Wang, S.; Claude, J.-P.; Streib, W. E.; Huffman, J. C.; Hendrickson, D. N.; Christou, G. *Inorg. Chem.* **1996**, *35*, 6450. (b) Wang, S. Y.; Huffman, J. C.; Folting, K.; Streib, W. E.; Lobkovsky, E. B.; Christou, G. *Angew. Chem., Int. Ed. Engl.* **1991**, *30*, 1672. (c) Kulawiec, R. J.; Crabtree, R. H.; Brudvig, G. W.; Gayle, K.; Schulte, G. K. *Inorg. Chem.* **1988**, *27*, 1309. (d) Wang, S.; Tsai, H.-L.; Folting, K.; Martin, J. D.; Hendrickson, D. N.; Christou, G. *J. Chem. Soc., Chem. Commun.* **1994**, 671. (e) Libby, E.; McCusker, J. K.; Schmitt, E. A.; Folting, K.; Hendrickson, D. N.; Christou, G. *Inorg. Chem.* **1991**, *30*, 3486. (f) Albela, B.; El Fallah, M. S.; Ribas, J.; Folting, K.; Christou, G.; Hendrickson, D. N. *Inorg. Chem.* **2001**, *40*, 1037. (g) Wang, S.; Tsai, H.-L.; Folting, K.; Streib, W. E.; Hendrickson, D. N.; Christou, G. *Inorg. Chem.* **1996**, *35*, 7578. (h) Aromí, G.; Bhaduri, S.; Artús, P.; Folting, K.; Christou, G., *Inorg. Chem.* **2002**, *41*, 805.

(8) (a) Wieghardt, K.; Bossek, U.; Nuber, B.; Weiss, J.; Bonvoisin, J.; Corbella, M.; Vitols, S. E.; Girerd, J. J. *J. Am. Chem. Soc.* **1988**, *110*, 7398. (b) Hagen, K. S.; Westmoreland, T. D.; Scott, M. J.; Armstrong, W. H. *J. Am. Chem. Soc.* **1989**, *111*, 1907. (c) Dube, C. E.; Wright, D. W.; Pal, S.; Bonitatebus, P. J.; Armstrong, W. H. *J. Am. Chem. Soc.* **1998**, *120*, 3704.

(9) Vincent, J. B.; Chang, H. R.; Folting, K.; Huffman, J. C.; Christou, G.; Hendrickson, D. N. *J. Am. Chem. Soc.* **1987**, *109*, 5703.

Table 1. Crystallographic Data for **1**·5MeCN and **2**·5MeCN

	1	**2**
empirical formula	$C_{90}H_{77}N_8O_{25}Mn_7$	$C_{102}H_{85}N_8O_{25}Mn_7$
fw	2055.18	2207.34
space group	$P\bar{1}$	*Pbca*
a, Å	15.9564(13)	27.695(2)
b, Å	16.5066(14)	22.430(2)
c, Å	20.5637(17)	30.293(3)
α, deg	110.824(2)	90
β, deg	110.666(2)	90
γ, deg	95.156(2)	90
V, Å^3	4590.8(7)	18818(3)
Z	2	8
T, K	173(2)	173(2)
radiation wavelength,[a] Å	0.71073	0.71073
ρ_{calcd}, g/cm^3	1.487	1.481
μ, mm^{-1}	1.010	1.244
R1[b,c]	0.0423	0.0574
wR2[d]	0.0871	0.1221

[a] Graphite monochromator. [b] $I > 2\sigma(I)$. [c] $R1 = 100\sum(||F_o| - |F_c||)/\sum|F_o|$. [d] $wR2 = 100[\sum[w(F_o^2 - F_c^2)^2]/\sum[w(F_o^2)^2]]^{1/2}$, $w = 1/[\sigma^2(F_o^2) + [(ap)^2 + bp]$, where $p = [\max(F_o^2, 0) + 2F_c^2]/3$.

X-ray Crystallography. Data were collected on a Siemens SMART PLATFORM equipped with a CCD area detector and a graphite monochromator utilizing Mo Kα radiation ($\lambda = 0.71073$ Å). Suitable crystals were attached to glass fibers using silicone grease and transferred to a goniostat where they were cooled to 173 K for data collection. An initial search of reciprocal space revealed a triclinic cell for **1** and an orthorhombic cell for **2**; the choice of space groups $P\bar{1}$, and *Pbca*, respectively, was confirmed by the subsequent solution and refinement of the structures. Cell parameters were refined using up to 8192 reflections. A full sphere of data (1850 frames) was collected using the *ω*-scan method (0.3° frame width). The first 50 frames were remeasured at the end of data collection to monitor instrument and crystal stability (the maximum correction on *I* was <1%). Absorption corrections by integration were applied on the basis of measured indexed crystal faces. The structures were solved by direct methods in SHELXTL6[10a] and refined on F^2 using full-matrix least squares. The non-H atoms were treated anisotropically, whereas the hydrogen atoms were placed in calculated, ideal positions and refined as riding on their respective carbon atoms.

For **1**·5MeCN, the asymmetric unit consists of the Mn_7 cluster and five MeCN molecules of crystallization. A total of 1176 parameters were included in the structure refinement on F^2 using 29290 reflections with $I > 2\sigma(I)$ to yield R1 and wR2 of 4.23% and 8.71%, respectively.

For **2**·5MeCN, the asymmetric unit consists of the Mn_7 cluster and five molecules of MeCN. The solvent molecules were disordered and could not be modeled properly; thus, program SQUEEZE,[10b] a part of the PLATON[10c] package of crystallographic software, was used to calculate the solvent disorder area and remove its contribution to the overall intensity data. A total of 1144 parameters were included in the structure refinement on F^2 using 21072 reflections with $I > 2\sigma(I)$ to yield R1 and wR2 of 5.74% and 12.21%, respectively.

Unit cell data and details of the structure refinements for complexes **1**·5MeCN and **2**·5MeCN are listed in Table 1.

Other Studies. Infrared spectra were recorded in the solid state (KBr pellets) on a Nicolet Nexus 670 FTIR spectrometer in the 400−4000 cm^{-1} range. Elemental analyses (C, H, and N) were performed by the in-house facilities of the University of Florida Chemistry Department. Variable-temperature dc and ac magnetic susceptibility data were collected at the University of Florida using a Quantum Design MPMS-XL SQUID susceptometer equipped with a 7 T magnet and operating in the 1.8−300 K range. Samples were embedded in solid eicosane to prevent torquing. Magnetization vs field and temperature data were fit using the program MAGNET.[11] Pascal's constants were used to estimate the diamagnetic corrections, which were subtracted from the experimental susceptibility to give the molar paramagnetic susceptibility (χ_M). Studies at ultralow temperatures (<1.8 K) were performed on single crystals at Grenoble using an array of micro-SQUIDs.[12] The high sensitivity of this magnetometer allows the study of single crystals on the order of 10−500 μm; the field can be applied in any direction by separately driving three orthogonal coils.

Results and Discussion

Syntheses. A common synthetic strategy for obtaining high-nuclearity Mn clusters is the reaction of a preformed Mn_x cluster with a bi-, tri-, or tetradentate chelate. Among the various Mn^{III} sources which have been explored in the past are $[Mn_3O(O_2CMe)_6(py)_3]$ (**3**; $2Mn^{III}$, Mn^{II}) and $(NBu^n_4)[Mn_4O_2(O_2CPh)_9(H_2O)]$ (**4**; $4Mn^{III}$), and they have proved useful routes to a variety of higher nuclearity complexes.[13,14] The tri- and tetradentate chelates we have used for such studies in the past have been fairly flexible ones, such as deprotonated *N*-methyldiethanolamine ($mdaH_2$) and triethanolamine ($teaH_3$), allowing the alkoxide arms to bind (and bridge) with little structural restriction, and thus giving a variety of products.[15] More recently, we began to address what would result if the much more rigid tridentate chelate terpy was employed. This and the related bidentate 2,2′-bipyridine (bpy) have been employed previously to limit nuclearity growth and have given several small nuclearity products, notable among which are the tetranuclear butterfly complexes with bpy[16] and the dimer-of-dimers[17] complexes with terpy, reported as potential models of the water-

(10) (a) Sheldrick, G. M. *SHELXTL6*; Bruker-AXS: Madison, WI, 2000. (b) van der Sluis, P.; Spek, A. L. *Acta Crystallogr.* **1990**, *A46*, 194. (c) Spek, A. L. *Acta Crystallogr.* **1990**, *A46*, C34.

(11) Davidson, E. R. MAGNET, Indiana University.

(12) Wernsdorfer, W. *Adv. Chem. Phys.* **2001**, *118*, 99.

(13) (a) Brechin, E. K. *Chem Commun.* **2005**, 5141. (b) Piligkos, S.; Rajaraman, G.; Soler, M.; Kirchner, N.; Slageren, J.; Bircher, R.; Parsons, S.; Gudel, H.-U.; Kortus, J.; Wernsdorfer, W.; Christou, G.; Brechin, E. K. *J. Am. Chem. Soc.* **2005**, *127*, 5572. (c) Boskovic, C.; Wernsdorfer, W.; Folting, K.; Huffman, J. C.; Hendrickson, D. N.; Christou, G. *Inorg. Chem.* **2002**, *41*, 5107. (d) Brechin, E. K.; Boskovic, C.; Wernsdorfer, W.; Yoo, J.; Yamaguchi, A.; Sanudo, E. C.; Concolino, T. R.; Rheingold, A. L.; Ishimoto, H.; Hendrickson, D. N.; Christou, G. *J. Am. Chem. Soc.* **2002**, *124*, 9710. (e) Mishra, A.; Wernsdorfer, W.; Abboud, K. A.; Christou, G. *J. Am. Chem. Soc.* **2004**, *126*, 15648.

(14) Mishra, A.; Wernsdorfer, W.; Abboud, K. A.; Christou, G. *Chem. Commun.* **2005**, 54.

(15) (a) Foguet-Albiol, D.; O'Brien, T. A.; Wernsdorfer, W.; Moulton, B.; Zaworotko, M. J.; Abboud, K. A.; Christou, G. *Angew. Chem., Int. Ed.* **2005**, *44*, 897. (b) Murugesu, M.; Wernsdorfer, W.; Abboud, K. A.; Christou, G. *Angew. Chem., Int. Ed.* **2005**, *44*, 792. (c) Bolcar, M. A.; Aubin, S. M. J.; Folting, K.; Hendrickson, D. N.; Christou, G. *Chem. Commun.* **1997**, 1485. (d) Harden, N. C.; Bolcar, M. A.; Wernsdorfer, W.; Abboud, K. A.; Streib, W. E.; Christou, G. *Inorg. Chem.* **2003**, *42*, 7067. (e) Boskovic, C.; Brechin, E. K.; Streib, W. E.; Folting, K.; Bollinger, J. C.; Hendrickson, D. N.; Christou, G. *J. Am. Chem. Soc.* **2002**, *124*, 3725. (f) Wittick, L.; Murray, K.; Moubaraki, B.; Batten, S.; Spiccia, L.; Berry, K. *Dalton Trans.* **2004**, 1003.

(16) Vincent, J. B.; Christmas, C.; Chang, H. R.; Li, Q.; Boyd, P. D. W.; Huffman, J. C.; Hendrickson, D. N.; Christou, G. *J. Am. Chem. Soc.* **1989**, *111*, 2086.

oxidizing complex of photosynthesis.[18,19] The present work arose from our belief that terpy might also be capable of producing higher nuclearity products than identified to date, and this turned out to be the case.

The synthetic procedure chosen involved the reaction of terpy with **3** and **4** in a Mn:terpy ratio of ~6:1 or higher to facilitate a high-nuclearity product. The mixed MeCN/ROH solvent mixture was necessary to ensure adequate solubility of all reagents, especially the terpy, and also led to alkoxide ligand incorporation; no isolable products were obtained when only MeCN was used. The reactions successfully gave products of formula $[Mn_7O_5(OR)_2(O_2CPh)_9(terpy)]$ (R = Me, CH_2Ph) in reasonable yield and with high purity and crystallinity. These preparations are summarized in eq 1

$$7[Mn_3O(O_2CPh)_6(py)_2(H_2O)] + 3terpy + H_2O + 6ROH \rightarrow 3[Mn_7O_5(OR)_2(O_2CPh)_9(terpy)] + 7py + 15PhCO_2H + 7pyH^+ + 7e^- \quad (1)$$

with **3** as the starting material. Charge considerations and bond valence sum (BVS) calculations establish that the product is mixed valent (Mn^{IV}, $5Mn^{III}$, and Mn^{II}) (vide infra) and the Mn^{IV} ion is likely generated by disproportionation of Mn^{III}, although eq 1 is simplified by showing the redox changes as metal oxidations.

The MeOH vs $PhCH_2OH$ reactions were designed to investigate whether the alcohol identity might alter the product, and for this we chose two that differed markedly in size and potentially in the solubility of their products. We thought this might lead to different Mn_x species crystallizing as relative solubilities of species in solution equilibrium with each other were altered. However, $PhCH_2OH$ and MeOH gave isostructural products. In some ways, this was slightly surprising, since we have often seen significant differences in product identity when identical reactions are run with different carboxylates, for example.[20] When EtOH was used, brown precipitates of manganese oxides/hydroxides were obtained, and no clean product could be isolated from the filtrate. If significantly more terpy was used, the same Mn_7 product was obtained, but it was contaminated with yellow crystals of terpy.

Description of the Structures. PovRay representations of the structure of **1** and its labeled core are presented in Figure 1. PovRay representations of the complete Mn_7 molecule of complex **2** and a stereopair are provided in Figure 2. Selected interatomic distances and angles for **1** and **2** are listed in Tables 2 and 3, respectively.

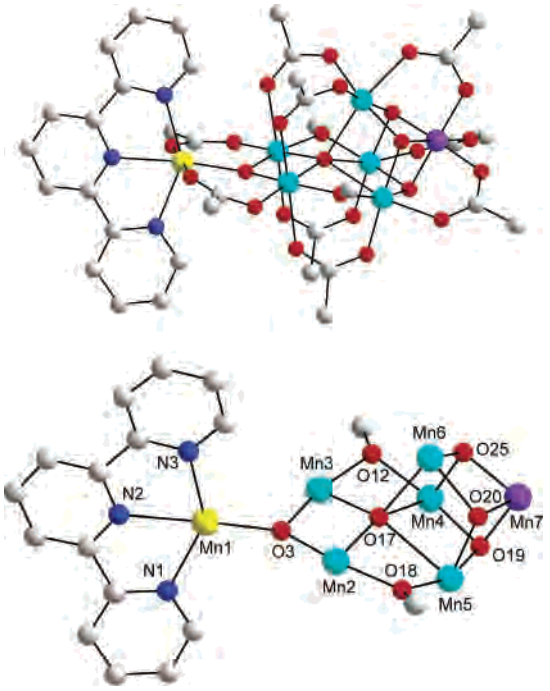

Figure 1. PovRay representations at the 50% probability level of (top) the structure of **1** (with the benzoate rings omitted for clarity except for the *ipso* C atoms) and (bottom) its labeled $[Mn_7O_5(OMe)_2(terpy)]^{9+}$ core. Color scheme: Mn^{IV}, purple; Mn^{III}, cyan; Mn^{II}, yellow; N, dark blue; O, red; C, gray. H atoms have been omitted for clarity.

Complex **1**·5MeCN crystallizes in the triclinic space group $P\bar{1}$. The $[Mn_7O_5(OMe)_2]^{9+}$ core can be described as a $[Mn^{IV}Mn^{III}{}_3O_4]$ cubane (Mn4, Mn5, Mn6, Mn7) fused with a $[Mn^{III}{}_3Mn^{II}O_2]$ butterfly (Mn1, Mn2, Mn3, Mn6) by sharing atoms Mn6 and O17 (Figure 1). There are thus four μ_3-O^{2-} ions and one μ_5-O^{2-} ion. Within this description, Mn2 and Mn3 are the "body" atoms of the butterfly and Mn1 and Mn6 are the "wingtip" atoms. Alternatively, the structure can be described as a $[Mn_4O_4]$ cubane linked via O17 to a $[Mn_3O]$ triangular unit. The two MeO^- groups, O12 and O18, bridge the cubane to the butterfly body Mn atoms. Charge considerations, inspection of bond distances, and the clear presence of Jahn−Teller (JT) distortions as expected for high-spin Mn^{III} in octahedral geometry establish the cluster as being mixed- and trapped-valent Mn^{IV}, $5Mn^{III}$, Mn^{II}. These metal oxidation states were confirmed quantitatively by bond valence sum (BVS) calculations (Table 4),[21] establishing Mn1 and Mn7 as the Mn^{II} and Mn^{IV} centers, respectively, of **1**. The terpy binds in its expected tridentate chelate fashion to Mn1, and the remaining peripheral ligation is provided by nine μ-benzoate groups in their common *syn*,*syn* bridging mode. Three benzoates bridge the three $Mn^{III}Mn^{IV}$ pairs within the cubane, four benzoates bridge cubane Mn^{III} and butterfly body Mn^{III} atoms, and two benzoates bridge butterfly body Mn^{III} atoms and the Mn^{II} atom. The tridentate terpy causes a significant deviation of the geometry at Mn1 from octahedral (N1−Mn1−N3 = 143.38(10)°, O3−Mn1−N3 = 116.08(9)°). The molecule has no crystallographic

(17) (a) Chen, H.; Faller, J. W.; Crabtree, R. H.; Brudvig, G. W. *J. Am. Chem. Soc.* **2004**, *126*, 7345. (b) Limburg, J.; Vrettos, J. S.; Chen, H.; de Paula, J. C.; Crabtree, R. H.; Brudvig, G. W. *J. Am. Chem. Soc.* **2001**, *123*, 423. (c) Chen, H. Y.; Collomb, M.-N.; Duboc, C.; Blondin, G.; Riviere, E.; Faller, J. W.; Crabtree, R. H.; Brudvig, G. W. *Inorg. Chem.* **2005**, *44*, 9567.

(18) Mukhopadhyay, S.; Mandal, S. K.; Bhaduri, S.; Armstrong, W. H. *Chem. Rev.* **2004**, *104*, 3981.

(19) (a) Yachandra, V. K.; Sauer, K.; Klein, M. P. *Chem. Rev.* **1996**, *96*, 2927. (b) Loll, B.; Kern, J.; Saenger, W.; Zouni, A.; Biesiadka, J. *Nature* **2005**, *438*, 1040. (c) Ferreira, K. N.; Iverson, T. M.; Maghlaoui, K.; Barber, J.; Iwata, S. *Science* **2004**, *303*, 1831.

(20) (a) King, P.; Wernsdorfer, W.; Abboud, K. A.; Christou, G. *Inorg. Chem.* **2004**, *43*, 7315. (b) Tasiopoulos, A. J.; Wernsdorfer, W.; Abboud, K. A.; Christou, G. *Inorg. Chem.* **2005**, *44*, 6324.

(21) (a) Brown, I. D.; Altermatt, D. *Acta. Crystallogr., Sect. B* **1985**, *41*, 244. (b) Liu, W.; Thorp, H. H. *Inorg. Chem.* **1993**, *32*, 4102. (c) Palenik, G. J. *Inorg. Chem.* **1997**, *36*, 4888.

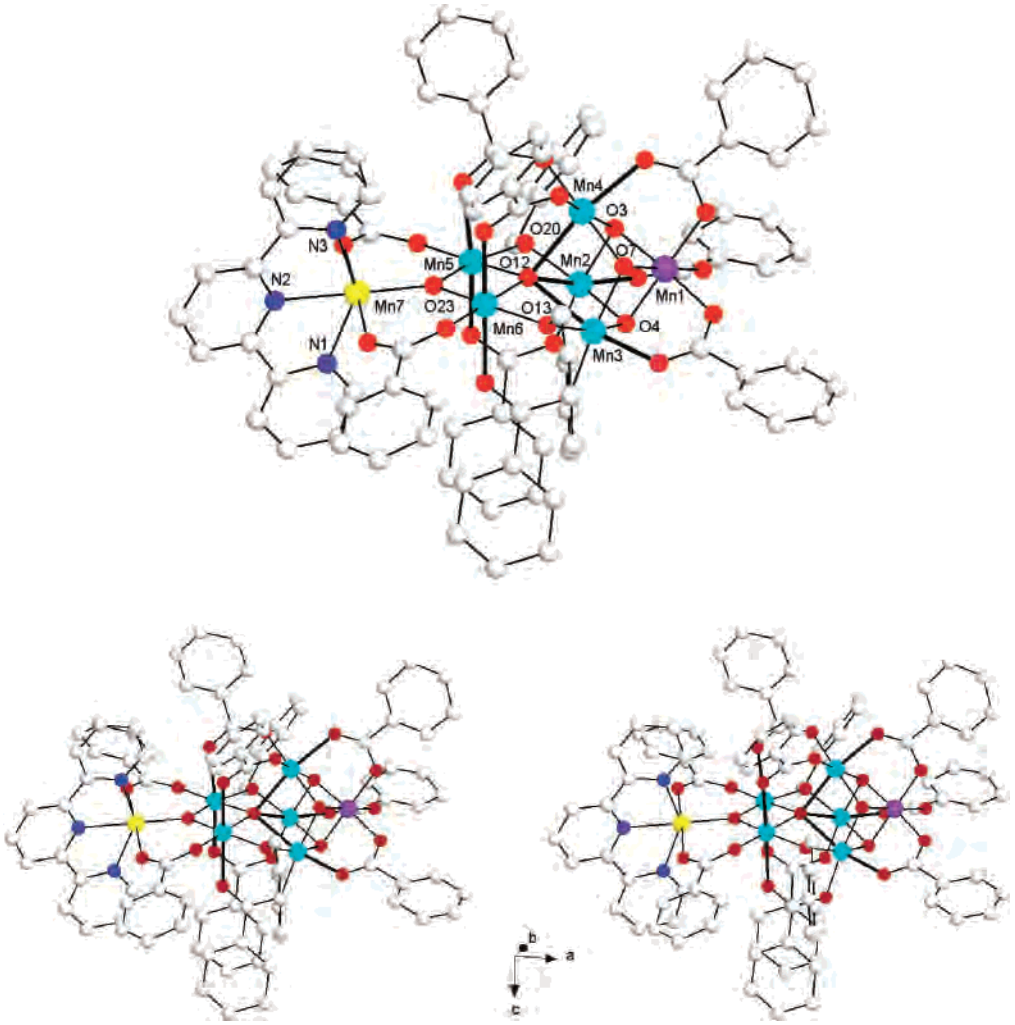

Figure 2. PovRay representations at the 50% probability level of (top) the labeled structure of **2** and (bottom) a stereopair. Color scheme: Mn^{IV}, purple; Mn^{III}, cyan; Mn^{II}, yellow; N, dark blue; O, red; C, gray. The thicker black bonds denote Jahn−Teller elongation axes. H atoms have been omitted for clarity.

symmetry, but has virtual C_s symmetry, with the mirror plane containing the terpy plane, Mn1, Mn7, and others (Figure 1).

Complex **2**·5MeCN crystallizes in the orthorhombic space group *Pbca* with the asymmetric unit containing the whole Mn_7 cluster. The structure of **2** (Figure 2) is very similar to that of **1**, the only difference being the benzyl vs methyl difference in the alkoxide groups. However, the ligand-induced core distortion is less profound for **2**, inasmuch as the butterfly portion of **2** encompassing Mn1 is nearly linear (O12−O23−Mn7 = 179° and O23−O12−Mn4 = 129° for the butterfly motif in Figure 2). The terpy is also more orthogonal to the rest of the core for **2**, with the corresponding O23−Mn7−N3 angle in Figure 2 being ∼104°, which is smaller than the corresponding 116° value mentioned earlier for complex **1**. This slight distortion in the core angles is undoubtedly caused by the bulk of the phenyl groups (when compared to the methyl groups of **1**) of the bridging phenyl methoxides.

All the Mn ions of **1** and **2** are six-coordinate with near-octahedral geometry except the Mn^{II} ion, which possess severely distorted octahedral geometry, as stated above. The five Mn^{III} ions display a JT distortion, and this takes the form of an axial elongation, with the JT-elongated bonds 0.1−0.3 Å longer than the other Mn^{III}−O bonds, as expected for high-spin Mn^{III} ions. The JT elongation axes are depicted in bold in Figure 2. The three in the cubane intersect at the μ_5-O^{2-} ion, and the two on the butterfly body atoms are parallel and perpendicular to the plane of the central rhombus of the butterfly. It should be noted that the cubane "fragment" of **1** and **2** is very similar to that of the discrete tetranuclear complexes with a $[Mn_4(\mu_3\text{-}O^{2-})_3(\mu_3\text{-}X^-)]^{6+}$ cubane core.[6a] These are also at the Mn^{IV}, $3Mn^{III}$ oxidation level, but with one vertex containing a monoanionic X^- (X^- = F^-, Cl^-, Br^-, MeO^-, HO^-, etc.) ion bridging the three Mn^{III} atoms, rather than an O^{2-} ion as in **1** and **2**. They also possess a bridging carboxylate between every $Mn^{IV}Mn^{III}$ pair, again as in **1** and **2**, and the three Mn^{III} JT axes also intersect at the triply bridging X^- ion.

The overall structures of **1** and **2** are very unusual and can be described as a fused butterfly/cubane or a linked triangle/cubane. We have in the past observed the transformation of a butterfly core to a cubane core by controlled potential electrolysis or disproportionation triggered by carboxylate abstraction,[6d,7g,h] so it is interesting to find a complex that is an amalgamation of both structural types.

Table 2. Selected Interatomic Distances (Å) and Angles (deg) for Complex **1**

Mn1−O3	2.048(2)	Mn7−O23	1.959(2)
Mn1−O2	2.163(2)	Mn6−Mn7	2.812(2)
Mn1−O4	2.167(2)	Mn4···Mn7	2.7908(7)
Mn1−N2	2.243(3)	Mn4···Mn5	3.1124(7)
Mn1−N	2.268(3)	Mn4···Mn6	3.1740(7)
Mn1−N3	2.273(3)	Mn5···Mn7	2.7894(7)
Mn2−O	1.842(2)	Mn5···Mn	3.1997(7)
Mn2−O17	1.925(1)	Mn6···Mn7	2.8127(7)
Mn2−O5	1.954(2)	Mn2···Mn	2.7898(7)
Mn2−O18	1.984(2)	Mn2···Mn5	3.0361(7)
Mn2−O8	2.205(2)	Mn3···Mn4	2.9958(7)
Mn2−O13	2.222(2)		
Mn3−O3	1.840(2)	O3−Mn1−O2	89.96(8)
Mn3−O17	1.936(1)	O3−Mn1−O4	92.21(8)
Mn3−O1	1.942(2)	O2−Mn1−O4	177.83(8)
Mn3−O12	1.987(2)	O3−Mn1−N2	168.47(9)
Mn3−O6	2.212(2)	O2−Mn1−N2	81.30(9)
Mn3−O10	2.231(2)	O4−Mn1−N2	96.54(9)
Mn6−O2	1.913(2)	O3−Mn1−N1	100.48(9)
Mn6−O7	1.931(2)	O2−Mn1−N1	87.96(10)
Mn6−O	1.933(2)	O4−Mn1−N1	91.63(9)
Mn6−O20	1.939(2)	N2−Mn1−N1	71.85(10)
Mn6−O2	2.193(2)	O3−Mn1−N3	116.08(9)
Mn6−O1	2.300(2)	O2−Mn1−N3	89.93(10)
Mn7−O19	1.840(2)	N2−Mn1−N3	71.69(10)
Mn7−O2	1.847(2)	N1−Mn1−N3	143.38(10)
Mn7−O2	1.860(2)	O3−Mn2−O17	84.57(8)
Mn7−O16	1.931(2)	O3−Mn2−O5	98.74(9)
Mn7−O21	1.941(2)	O17−Mn2−O5	176.68(9)

Table 3. Selected Interatomic Distances (Å) and Angles (deg) for Complex **2**

Mn7−O2	2.035(2)	Mn1−O5	1.960(3)
Mn7−O25	2.170(3)	Mn1···Mn3	2.7787(8)
Mn7−O22	2.192(3)	Mn1···Mn2	2.8028(9)
Mn7−N	2.249(4)	Mn1···Mn4	2.8090(8)
Mn7−N3	2.259(4)	Mn2···Mn5	3.0088(8)
Mn7−N	2.276(5)	Mn2···Mn3	3.0624(9)
Mn3−O13	1.887(3)	Mn2···Mn4	3.1528(9)
Mn3−O4	1.912(3)	Mn3···Mn6	3.0020(9)
Mn3−O1	1.923(3)	Mn3···Mn4	3.2031(9)
Mn3−O7	1.926(3)	Mn5···Mn6	2.8013(9)
Mn3−O6	2.105(3)		
Mn3−O12	2.407(3)	O23−Mn7−O22	90.90(11)
Mn4−O14	1.896(3)	O25−Mn7−O22	177.29(13)
Mn4−O3	1.906(3)	O23−Mn7−N2	172.24(13)
Mn4−O7	1.924(3)	O25−Mn7−N2	82.71(12)
Mn4−O1	1.934(3)	O22−Mn7−N2	95.62(12)
Mn4−O9	2.161(3)	O23−Mn7−N3	104.08(13)
Mn4−O12	2.366(3)	O25−Mn7−N3	90.89(14)
Mn2−O18	1.910(3)	O22−Mn7−N3	90.61(13)
Mn2−O4	1.914(3)	N2−Mn7−N3	71.73(16)
Mn2−O20	1.915(3)	Mn1−O3−Mn2	94.81(11)
Mn2−O3	1.940(3)	Mn4−O3−Mn2	110.10(11)
Mn2−O2	2.140(3)	Mn1−O4−Mn3	95.04(12)
Mn2−O12	2.307(2)	Mn1−O4−Mn2	96.04(12)
Mn1−O4	1.856(3)	Mn3−O4−Mn2	106.35(12)
Mn1−O	1.860(3)	O21−Mn5−O19	84.19(11)
Mn1−O3	1.867(3)	O20−Mn5−O19	82.96(11)
Mn1−O8	1.926(3)	O15−Mn5−O19	167.31(11)
Mn1−O1	1.960(3)	O23−Mn5−Mn6	40.73(8)

Additionally, the fact that the complex contains three Mn oxidation states is also very rare, with previous examples including Mn_3,[22] Mn_4,[23] Mn_{13},[24] Mn_{25},[25] Mn_{30},[26] and reduced Mn_{12}[27] complexes, to name a few.

A few other Mn_7 complexes have been reported in the literature. Among these are the $4Mn^{II}$, $3Mn^{III}$ complexes consisting of a Mn_6 hexagon of alternating Mn^{II} and Mn^{III} ions surrounding a central Mn^{II} ion.[15b,c] A Mn_7 complex with a similar core but instead consisting of $3Mn^{II}$ and $4Mn^{III}$ has also been reported.[28] However, more structurally relevant to **1** and **2** are (i) a Mn_7 complex that can be described as two $[Mn_4O_2]$ butterfly units fused together by sharing a common Mn atom[29] and (ii) two Mn_4 cubanes fused together by a shared Mn ion.[30]

Table 4. Bond Valence Sums for the Mn Atoms in **1** and **2**[a]

	1			**2**		
atom	Mn^{II}	Mn^{III}	Mn^{IV}	Mn^{II}	Mn^{III}	Mn^{IV}
Mn(1)	*2.13*	2.00	2.01	4.14	3.79	*3.98*
Mn(2)	3.20	*2.93*	3.08	3.23	*2.95*	3.09
Mn(3)	3.20	*2.92*	3.07	3.27	*2.99*	3.14
Mn(4)	3.22	*2.95*	3.09	3.21	*2.94*	3.08
Mn(5)	3.20	*2.93*	3.08	3.10	*2.84*	2.98
Mn(6)	3.12	*2.85*	2.99	3.18	*2.91*	3.05
Mn(7)	4.24	3.88	*4.07*	*2.12*	1.99	2.00

[a] The italic value is the one closest to the charge for which it was calculated. The oxidation state of a particular atom can be taken as the whole number nearest to the italic value.

dc Magnetic Susceptibility Studies. Solid-state variable-temperature magnetic susceptibility measurements were performed on vacuum-dried microcrystalline samples of complexes **1** and **2** suspended in eicosane to prevent torquing. The dc magnetic susceptibility (χ_M) data were collected in the 5.0−300 K range in a 0.1 T magnetic field and are plotted as $\chi_M T$ vs T in Figure 3. For **1**, the $\chi_M T$ value of 16.91 cm^3 mol^{-1} K at 300 K decreases slightly to 15.21 at 50 K, and then it steadily increases with decreasing temperature to reach 17.83 cm^3 mol^{-1} K at 5.0 K. The $\chi_M T$ value of complex **2** is very similar to that of **1**, with a value of 16.66 cm^3 mol^{-1} K at 300 K which decreases slightly to 15.46 at 50 K and then increases with decreasing temperature to 17.48 cm^3 mol^{-1} K at 5.0 K. The spin-only ($g = 2$) value for one Mn^{IV}, five Mn^{III}, and one Mn^{II} noninteracting ions is 21.25 cm^3 mol^{-1} K, so the 300 K values indicate dominant antiferromagnetic exchange interactions. However, the increase in $\chi_M T$ below 50 K indicates the lowest lying spin states are nevertheless of significant magnitude. In fact, the lowest temperature data at <10 K are indicative of an increasing population of a rather large ground-state spin for the two complexes; the values at 5.0 K suggest $S = 6$, whose spin-only ($g = 2$) value would be 21 cm^3 mol^{-1} K. The observed values at

(22) Mukherjee, C.; Weyhermüller, T.; Wieghardt, K.; Chaudhuri, P. *Dalton Trans.* **2006**, 2169.

(23) (a) Chan, M. K.; Armstrong, W. H. *J. Am. Chem. Soc.* **1990**, *112*, 4985. (b) Suzuki, M.; Senda, H.; Suenaga, M.; Sugisawa, T.; Uehara, A. *Chem. Lett.* **1990**, 923.

(24) Sun, Z.; Gantzel, P. K.; Hendrickson, D. N. *Inorg. Chem.* **1996**, *35*, 6640.

(25) Murugesu, M.; Habrych, M.; Wernsdorfer, W.; Abboud, K. A.; Christou, G. *J. Am. Chem. Soc.* **2004**, *126*, 4766.

(26) Soler, M.; Wernsdorfer, W.; Folting, K; Pink, M.; Christou, G. *J. Am. Chem. Soc.* **2004**, *126*, 2156.

(27) (a) Eppley, H. J.; Tsai, H.-L.; Vries, N.; Folting, K.; Christou, G.; Hendrickson, D. N. *J. Am. Chem. Soc*. **1995**, *117*, 301. (b) Aubin, S. M. J.; Sun, Z.; Pardi, L.; Krzystek, J.; Folting, K.; Brunel, L.-C.; Rheingold, A. L.; Christou, G.; Hendrickson, D. N. *Inorg. Chem.* **1999**, *38*, 5329. (c) Soler, M.; Wernsdorfer, W.; Abboud, K. A.; Huffman, J. C.; Davidson, E. R.; Hendrickson, D. N.; Christou, G. *J. Am. Chem. Soc*. **2003**, *135*, 3576.

(28) Abbati, G. L.; Cornia, A.; Fabretti, A. C.; Caneschi, A.; Gatteschi, D. *Inorg. Chem.* **1998**, *37*, 3759.

(29) Bhula, R.; Weatherburn, D. C. *Angew. Chem., Int. Ed.* **1991**, *30*, 688.

(30) Clerk, M. D.; Zaworotko, M. J. *Chem. Commun*. **1991**, 1607.

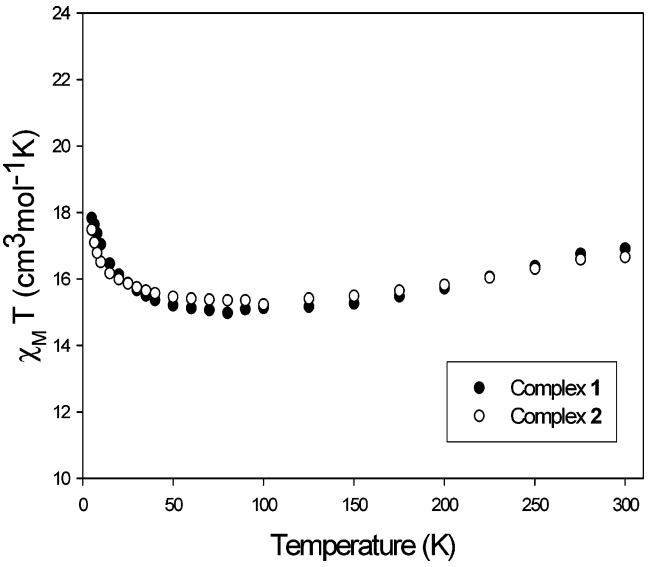

Figure 3. $\chi_M T$ vs T for complexes **1** and **2**.

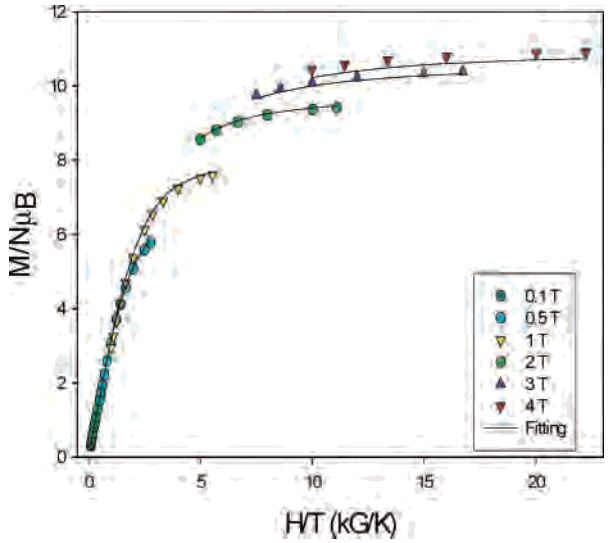

Figure 4. Magnetization (M) vs field (H) and temperature (T) data, plotted as reduced magnetization ($M/N\mu_B$) vs H/T, for complex **1** at applied fields of 0.1−4 T and in the 1.8−10 K temperature range. The solid lines are the fits of the data; see the text for the fit parameters.

5.0 K thus suggest $S = 6$ and $g \approx 1.84$ for **1** and $S = 6$ and $g \approx 1.82$ for **2**, as expected for Mn, whose g values are slightly less than 2.0.

The nuclearity, low symmetry, and large number of exchange interactions of the molecules (eight under C_s virtual symmetry) make a matrix diagonalization method to evaluate the various Mn_2 pairwise exchange parameters (J_{ij}) onerous and also rule out application of the equivalent operator approach based on the Kambe vector coupling method.[31] We therefore focused instead on determining only the ground-state S, the axial ZFS parameter D, and the electronic g factors for **1** and **2**. Hence, magnetization (M) data were collected in the magnetic field and temperature ranges 0.1−4 T and 1.8−10 K. The data are plotted as reduced magnetization ($M/N\mu_B$) versus H/T in Figures 4 and 5 for **1** and **2**, respectively. For a spin system occupying only the ground

(31) Kambe, K. *J. Phys. Soc. Jpn.* **1950**, *48*, 15.

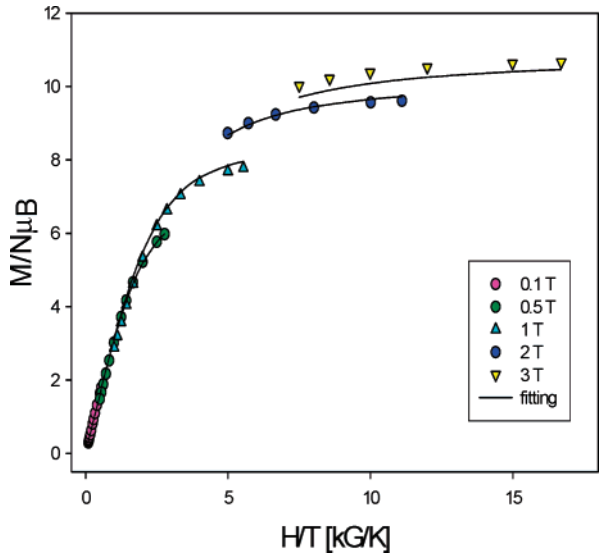

Figure 5. Magnetization (M) vs field (H) and temperature (T) data, plotted as reduced magnetization ($M/N\mu_B$) vs H/T, for complex **2** at applied fields of 0.1−3 T and in the 1.8−10 K temperature range. The solid lines are the fits of the data; see the text for the fit parameters.

state and experiencing no ZFS, the various isofield lines would be superimposed and $M/N\mu_B$ would saturate at a value of gS.[32] The nonsuperimposition of the isofield lines in Figures 4 and 5 thus indicates the presence of ZFS. The data were fit, using the program MAGNET,[11] by diagonalization of the spin Hamiltonian matrix assuming only the ground state is populated, incorporating axial anisotropy (DS_z^2) and Zeeman terms and employing a full powder average. The magnetization fit thus modeled each complex as a "giant spin" with Ising-like anisotropy. The corresponding spin Hamiltonian is given by eq 2,

$$\mathscr{H} = DS_z^2 + g\mu_B\mu_0 SH \qquad (2)$$

where μ_B is the Bohr magneton, S_z is the easy-axis spin operator, g is the electronic g factor, μ_0 is the vacuum permeability, and H is the applied field. The last term in eq 2 is the Zeeman energy associated with an applied magnetic field. For **1**, the fit (solid lines in Figure 4) gave $S = 6$, $D = -0.22$ cm^{-1}, and $g = 1.88$. Data for fields higher than 4 T were excluded to avoid possible problems from low-lying excited states. For complex **2**, a satisfactory fit could only be obtained if the 4 T data were also excluded, presumably due to excited states, and thus, only the data collected in the 0.1−3 T field range are shown in Figure 5. The fit (solid lines in Figure 5) gave $S = 6$, $D = -0.18$ cm^{-1}, and $g = 1.86$. The obtained fit parameters for **1** and **2** are in satisfying agreement with the approximate conclusions from the $\chi_M T$ vs T data described above. The general conclusion is that antiferromagnetic exchange dominates within the Mn_7 core, but the exact ground-state spin alignments are such as to result in a relatively large net spin of $S = 6$. A qualitative rationalization of the latter will be provided below. The small

(32) (a) Aromi, G.; Wemple, M. W.; Aubin, S. M. J.; Folting, K.; Hendrickson, D. N.; Christou, G. *J. Am. Chem. Soc.* **1998**, *120*, 2977. (b) Aromi, G.; Knapp, M. J.; Claude, J.-P.; Huffman, J. C.; Hendrickson, D. N.; Christou, G. *J. Am. Chem. Soc.* **1999**, *121*, 5489.

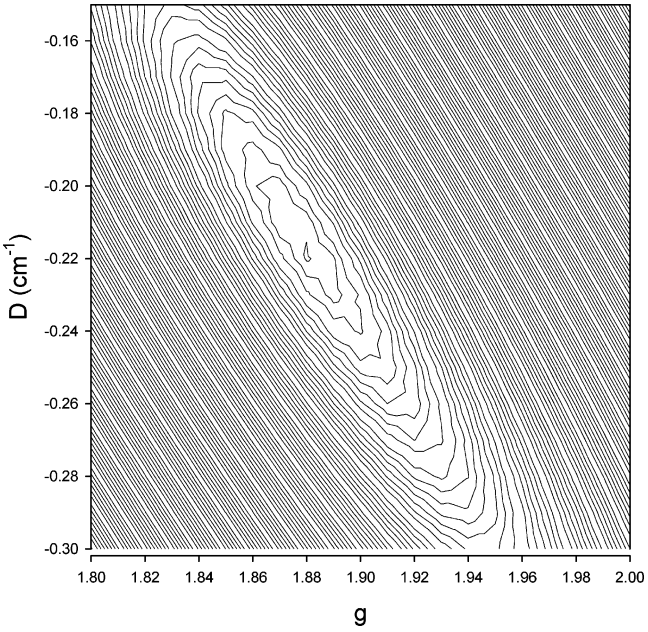

Figure 6. Two-dimensional contour plot of the root-mean-square error surface for the D vs g fit for complex **1**.

but nonzero D values of **1** and **2** are consistent with the fact that the JT axes of the Mn^{III} atoms, whose single-ion anisotropies are the main source of the molecular anisotropy (D), are not randomly oriented (Figure 2) and thus yield a nonzero molecular resultant.

To confirm that the obtained fit parameters were the true global rather than local minima, we examined the root-mean square D vs g error surfaces for the fits, calculated using the program GRID.[33] The obtained error surface for **1** is shown in Figure 6 as a two-dimensional contour plot for the $D = -0.15$ to -0.30 cm^{-1} and $g = 1.8-2.0$ ranges. Only one minimum is observed in this range, and this is a fairly well-defined minimum, indicating a fairly small level of uncertainty in the best-fit parameters. The two lowest error contour lines cover a range of $D \approx -0.20$ to -0.23 cm^{-1} and $g \approx 1.87-1.89$, giving fit values and their uncertainties of $D = -0.22(1)$ cm^{-1} and $g = 1.88(1)$. Similar observations are made for complex **2**, although in this case the minimum is somewhat shallower and there is a correspondingly slightly greater level of uncertainty, giving $D = -0.18(2)$ cm^{-1} and $g = 1.86(2)$. Note, however, that the error surface indicates the precision of the fit minima, not the accuracy of the obtained D and g parameters; bulk magnetization data are not in general the most accurate way to obtain these, more sensitive techniques such as EPR being superior for this purpose.

Rationalization of the $S = 6$ Ground State. Although **1** and **2** possess a complicated, low-symmetry Mn_7 core, their $S = 6$ ground states can nevertheless be rationalized in a very satisfying manner (Figure 7). This is achieved using the known spin coupling pattern in the discrete Mn_4 complexes mentioned earlier that possess the same Mn^{IV}, $3Mn^{III}$ cubane core found within **1** and **2**. These Mn_4 complexes of C_{3v} symmetry exhibit ferromagnetic and antiferromagnetic exchange interactions within the $Mn^{III}Mn^{III}$ and $Mn^{IV}Mn^{III}$ pairs, respectively.[6] As a result the ground state is $S = 9/2$, due to the three Mn^{III} ($S = 2$) spins being parallel to each other and antiparallel to the Mn^{IV} ($S = 3/2$) spin. Assuming (very reasonably) that the same situation exists for this cubane unit within the larger Mn_7 core of **1** and **2**, the question then becomes how this $S = 9/2$ unit couples to the other Mn atoms. Inspection of Figure 1 shows that the primary exchange pathways between the cubane Mn^{III} atoms and the butterfly body Mn^{III} atoms (Mn2 and Mn3) are via the μ_5-O^{2-} ion (O17) and the μ-MeO^- groups (O12 and O18). Remembering that (i) the Mn^{III} JT axes define the local Mn z axes and (ii) the cubane Mn^{III} JT axes intersect at O17 whereas those for body Mn^{III} atoms include neither O17 nor O12/O18, then Mn−O−Mn $d_\sigma-p_\sigma-d_\sigma$ exchange pathways through O17 and O12/O18 atoms will involve a singly occupied d_{z^2} orbital on cubane Mn^{III} atoms and an empty $d_{x^2-y^2}$ orbital on body Mn^{III} atoms. These pathways would thus be expected to give ferromagnetic contributions to the total exchange between these metals. Notwithstanding Mn−O−Mn $d_\pi-p_\pi-d_\pi$ exchange pathways involving singly occupied Mn d_π orbitals that would be expected to give antiferromagnetic contributions, it is concluded that there are overall ferromagnetic exchange interactions between the cubane and butterfly body Mn^{III} atoms in **1** and **2**. The same was observed for the ferromagnetically coupled $[Mn_6O_4X_4(dbm)_6]$ (X = Cl, Br) complexes with an $S = 12$ ground state, whose ferromagnetic coupling between Mn^{III} atoms was rationalized in the same fashion as for **1** and **2**.[32] Finally, it is expected that the exchange interactions between the butterfly body Mn^{III} atoms and the Mn^{II} atom will be antiferromagnetic, as they are in the discrete Mn_4 butterfly complexes,[7] so the ground states of **1** and **2** are concluded to comprise all the Mn^{III} spins being parallel to each other and antiparallel to the Mn^{II} and Mn^{IV} spins, giving a predicted ground state of $S = 10 - 5/2 - 3/2 = 6$, as observed experimentally. This is summarized in Figure 7.

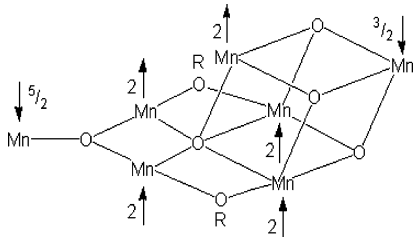

Figure 7. Schematic representation of the Mn spin alignments giving the $S = 6$ ground state for Mn_7 complexes **1** and **2**.

ac Magnetic Susceptibility Studies on Complexes 1 and 2. The $S = 6$ ground state of **1** and **2** coupled with $D \approx -0.2$ cm^{-1} was thought to possibly provide a big enough barrier for magnetization reversal, perhaps making these complexes SMMs. As stated earlier, the upper limit to this barrier is given by $U = S^2|D|$ for integer spins,[1] which computes to 7.9 and 6.5 cm^{-1} for **1** and **2**, respectively, but the true or effective barrier U_{eff} would be significantly smaller due to QTM through upper regions of the barrier. Whether the U_{eff} would thus be large enough to result in slow

(33) Davidson, E. R. GRID, Indiana University.

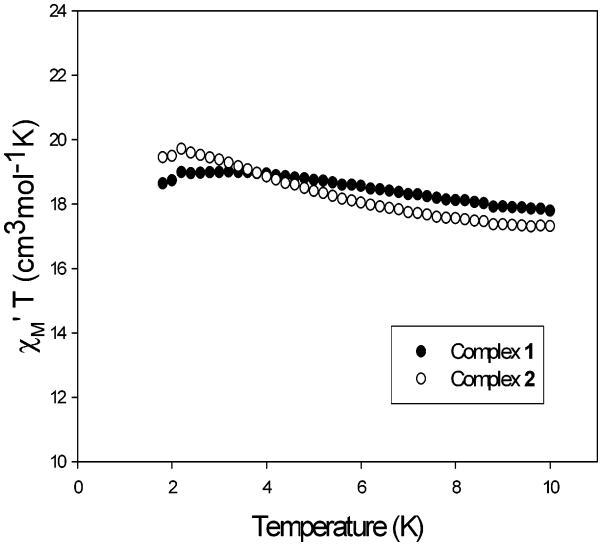

Figure 8. In-phase ac susceptibility signals, $\chi_M'T$ vs T, for complexes **1** and **2**.

relaxation at low temperatures was therefore explored by ac magnetic susceptibility studies. These studies also provided additional support for the $S = 6$ ground state.

ac studies were performed on vacuum-dried microcrystalline samples of **1** and **2** in the temperature range 1.8−10 K with a zero dc field and a 3.5 G ac field oscillating at frequencies in the 5−1000 Hz range. The in-phase (χ_M') component of the ac susceptibility, plotted as $\chi_M'T$ vs T, is shown in Figure 8 for complexes **1** and **2**; there were no out-of-phase ac signals down to 1.8 K, the operating limit of our SQUID susceptometer. ac susceptibility studies use no dc field and thus avoid any possible complications from low-lying excited states with larger S values than the ground state, whose M_S components could cross with those of the ground state in an applied dc field. As we have described in multiple previous reports,[4e,f,26,34,35] ac studies are thus an invaluable way to obtain (or confirm) the ground-state S. This is done by extrapolating the $\chi_M'T$ value to 0 K (from temperatures where the data are unaffected by slow magnetization relaxation or weak intermolecular interactions), where only the ground state will be populated. The $\chi_M'T$ of complex **1** is 17.79 $cm^3\ mol^{-1}$ K at 10 K, increases steadily to a plateau of 18.64 $cm^3\ mol^{-1}$ K at ∼2 K, and then drops very slightly. Similarly, the $\chi_M'T$ for **2** of 17.32 $cm^3\ mol^{-1}$ K at 10 K increases to 19.71 $cm^3\ mol^{-1}$ K at ∼2 K and then drops very slightly. The increasing $\chi_M'T$ with decreasing temperature is consistent with a decreasing population of excited states with smaller spin than the ground state. Taking the plateau values as the extrapolation, this gives $S = 6$ and $g = 1.88$ for **1** and $S = 6$ and $g = 1.9$ for **2**. These are in satisfying agreement with the S and g values obtained from the dc magnetization fits (vide supra). Note that $S = 5$ or 7 would give $\chi_M'T$ of 15 and 28 $cm^3\ mol^{-1}$ K (for $g = 2$), clearly very different from the experimental numbers.

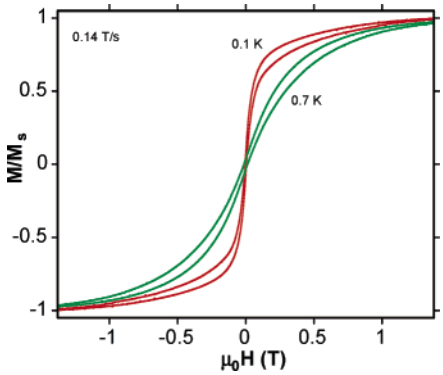

Figure 9. Magnetization (M) vs applied magnetic field (H) hysteresis loops for **2** at temperatures of 0.7 and 0.1 K and at a 0.14 T/s sweep rate. M is normalized to its saturation value, M_s.

Hysteresis Studies below 1.8 K. Since $\chi_M'T$ showed no (significant) decrease down to 1.8 K, the complexes clearly did not exhibit the slow magnetization relaxation that is suggestive of an SMM. This was supported by the absence of an out-of-phase ac susceptibility signal (χ_M'') for the frequency range examined. To explore whether slow relaxation might nevertheless be manifested at even lower temperatures, magnetization vs dc field scans were carried out on a single crystal of **2**·5MeCN using a micro-SQUID apparatus.[12] The observation of hysteresis loops in such studies represents the diagnostic property of a magnet, including SMMs and superparamagnets below their blocking temperature (T_B). In particular, the hysteresis loops of SMMs exhibit increasing coercivities with increasing sweep rates and with decreasing temperatures.

The magnetization vs dc field sweeps at a fixed sweep rate of 0.14 T/s and at temperatures of 0.7 and 0.1 K are presented in Figure 9. The 0.7 K scan displays an apparently greater coercivity than the 0.1 K scan, but that must be due to the former being a result of a phonon bottleneck rather than a significant barrier. The 0.1 K scan does show a very small amount of hysteresis, evident at non-zero-field positions, but this is truly very small. We conclude from this that despite a predicted barrier U of ∼7 cm^{-1} calculated from $S^2|D|$, it is clear that the true barrier U_{eff} is much smaller due to fast QTM. The latter is responsible for the large step (magnetization change) at zero field that effectively relaxes almost all the magnetization and allows only a very small hysteresis at non-zero-field values. Large QTM rates would be consistent with the low symmetry of the molecule, which would result in a significant transverse anisotropy (rhombic ZFS parameter, E). The latter will result in significant mixing of states on either side of the anisotropy barrier and thus significant QTM rates. Note that the fast QTM rates also preclude obtaining magnetization decay vs time data with which to construct an Arrhenius plot to determine the U_{eff} and τ_0 values. We conclude that complexes **1** and **2** are not SMMs.

Summary and Conclusions

The use of terpy in reactions with certain Mn_3 and Mn_4 species has led to an interesting new structural type in manganese carboxylate cluster chemistry that can be de-

(34) (a) King, P.; Wernsdorfer, W.; Abboud, K. A.; Christou, G. *Inorg. Chem.* **2005**, *44*, 8659. (b) Foguet-Albiol, D.; Abboud, K. A.; Christou, G. *Chem. Commun.* **2005**, 4282.
(35) Mishra, A.; Abboud, K. A.; Christou, G. *Inorg. Chem.* **2005**, *45*, 2364.

scribed as a hybrid of two previously observed cores. It is also a rare example of three different Mn oxidation states in the same unit. The obtained complexes possess $S = 6$ ground states, and it is satisfying that this can be rationalized by qualitative considerations of the expected Mn_2 pairwise couplings. The low anisotropy, however, as reflected in the small D values, as well as the low C_1 (virtual C_s) symmetry, means that these complexes are not new additions to the family of SMMs. Nevertheless, they are interesting new additions to the family of Mn_x clusters. The preparations of **1** and **2** are obviously dependent on the presence of terpy in the reaction, but only one terpy is incorporated into the structure, and then only on the Mn^{II} atom on the periphery of the molecule and not apparently of much importance to the topology of the remaining Mn_6 portion of the structure. In fact, with hindsight, there seems no reason this type of structure could not have been previously encountered with other chelates such as bpy and a monodentate ligand (H_2O, Cl^-, etc.) in place of terpy. Of course, this merely emphasizes how complicated and unpredictable are the precise nuclearities and topologies of products of such labile and complicated multicomponent reactions under thermodynamic control.

Acknowledgment. We thank the National Science Foundation for support of this work.

Supporting Information Available: X-ray crystallographic data in CIF format for complexes **1**·5MeCN and **2**·5MeCN. This material is available free of charge via the Internet at http://pubs.acs.org.

IC061334D